

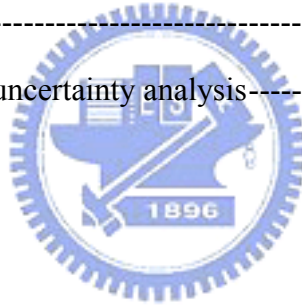
TABLE OF CONTENTS

ABSTRACT	i
TABLE OF CONTENTS	iii
LIST OF TABLE	v
LIST OF FIGURE	vi
NOMENCLATURE	xiv
CHAPTER 1 INTRODUCTION	1
1.1 Motive of the Present Study	1
1.2 Literature Review - Heat Transfer Performance, Bubble Characteristics, and Enhanced Surface Micro-structures	2
1.2.1 Single-phase Convective Heat Transfer	2
1.2.2 Two-phase Heat Transfer Performance	3
1.2.3 Bubble Characteristics	5
1.2.4 Enhanced Surface Micro-structures	7
1.3 Review of Correlation Equations for Two Phase Flow Boiling Heat Transfer	9
1.4 Objective of This Study	11
CHAPTER 2 EXPERIMENTAL APPARATUS AND PROCEDURES	18
2.1 Degassing Unit	18
2.2 Coolant Loop	18
2.3 Test Section	20
2.4 Hot-water Loop	21
2.5 Cold-water Loop	22
2.6 DC Power Supply	22
2.7 Data Acquisition	23
2.8 Optical Measurement Technique	23
2.9 Experimental Procedures	24
2.10 Experimental Parameters	24
CHAPTER 3 DATA REDUCTION	36

3.1 Single Phase Heat Transfer	36
3.2 Two Phase Flow Boiling Heat Transfer	38
3.3 Uncertainty Analysis	39
CHAPTER 4 SATURATED FLOW BOILING OF FC-72 ON A HEADED MICRO PIN-FINDED SILICON CHIP FLUSH MOUNTED ON BOTTOM OF RECTANGULAR CHANNEL	41
4.1 Single-phase Liquid Convective Heat Transfer	41
4.2 Saturated Flow Boiling Curves	43
4.3 Saturated Flow Boiling Heat Transfer Coefficients	44
4.4 Bubble Characteristics	45
4.5 Correlation Equations	47
4.6 Concluding Remarks	51
CHAPTER 5 SUBCOOLED FLOW BOILING OF FC-72 ON A HEADED MICRO PIN-FINDED SILICON CHIP FLUSH MOUNTED ON BOTTOM OF RECTANGULAR CHANNEL	78
5.1 Subcooled Flow Boiling Curves	78
5.2 Subcooled Flow Boiling Heat Transfer Coefficients	81
5.3 Bubble Characteristics	81
5.4 Correlation Equations	84
5.5 Concluding Remarks	88
CHAPTER 6 CONCLUDING REMARKS	147
REFERENCES	149

LIST OF TABLE

Table 1.1	Thermodynamic properties for FC-72 -----	12
Table 1.2	Some single-phase convection heat transfer correlations for electronic cooling -----	13
Table 1.3	Some flow boiling two-phase heat transfer correlations for electronic cooling -----	14
Table 1.4	Correlations for bubble departure diameter in flow boiling-----	15
Table 1.4	Continued -----	16
Table 1.5	Correlations for heat transfer & active nucleation site density in flow boiling-----	17
Table 2.1	Experimental parameters-----	26
Table 2.2	Thermodynamic and transport properties of the dielectric refrigerant FC-72 list -----	27
Table 3.1	Summary of the uncertainty analysis-----	40



LIST OF FIGURES

Experiment Apparatus

Fig 2.1	Schematic diagram of experimental apparatus -----	28
Fig 2.2	Three-dimensional plots of test section along with inlet and outlet sections -----	29
Fig 2.3	Three-dimensional plots illustrating the test section in the rectangular flow-channel -----	30
Fig 2.4	Three-dimensional pictures showing (a) hollow cylindrical Teflon block and (b) cylindrical Teflon bolt -----	31
Fig 2.5	Locations of thermocouples -----	32
Fig 2.6	Schematics of the silicon chip module -----	33
Fig 2.7	Flow chart for the micro pin-fins fabrication -----	34
Fig 2.8	Photographs of micro-pin-fins on the silicon chip taken by SEM -----	35

Saturated Flow Boiling

Fig. 4.1	Comparison of the present single-phase liquid convection heat transfer data for the chip with a smooth surface with the correlation of Gersey and Mudawar (1992) for (a) $h_{1\phi}$ vs. G and (b) Nu_L vs. Re_L -----	53
Fig. 4.2	Effects of the micro pin-fins on single-phase liquid convective heat transfer coefficients at $T_{in} = 25$ °C for (a) $h_{1\phi}$ vs. G and (b) Nu_L vs. Re_L -----	54
Fig. 4.3	Boiling curves for various coolant mass fluxes for $T_{sat} = 54.3$ °C for the chip with (a) smooth surface and (b) pin-finned 200 surface and (c) pin-finned 100 surface -----	55
Fig. 4.4	Boiling curves for various micro-structures of chip surface for $T_{sat} = 54.3$ °C at (a) $G = 287$ kg/m ² s and (b) $G = 431$ kg/m ² s -----	56
Fig. 4.5	Saturated flow boiling heat transfer coefficients for various coolant mass fluxes for $T_{sat} = 54.3$ °C for the chip with (a) smooth surface and (b) pin-finned 200 surface and (c) pin-finned 100 surface -----	57
Fig. 4.6	Saturated flow boiling heat transfer coefficients for various micro-structures of chip surface for $T_{sat} = 54.3$ °C at (a) $G = 287$ kg/m ² s and (b) $G = 431$ kg/m ² s -----	58

Fig. 4.7	Photos of boiling flow for various imposed heat fluxes for chip with smooth surface for (a) $G = 287 \text{ kg/m}^2\text{s}$ and (b) $G = 431 \text{ kg/m}^2\text{s}$ -----	59
Fig. 4.8	Photos of boiling flow for various imposed heat fluxes for chip with pin-finned 200 surface for (a) $G = 287 \text{ kg/m}^2\text{s}$ and (b) $G = 431 \text{ kg/m}^2\text{s}$ -----	60
Fig. 4.9	Photos of boiling flow for various imposed heat fluxes for chip with pin-finned 100 surface for (a) $G = 287 \text{ kg/m}^2\text{s}$ and (b) $G = 431 \text{ kg/m}^2\text{s}$ -----	61
Fig. 4.10	Mean bubble departure diameters for various coolant mass fluxes for $T_{\text{sat}} = 54.3 \text{ }^\circ\text{C}$ for the chip with (a) smooth surface and (b) pin-finned 200 surface and (c) pin-finned 100 Surface-----	62
Fig. 4.11	Mean bubble departure diameters for various micro-structures of chip surface for $T_{\text{sat}} = 54.3 \text{ }^\circ\text{C}$ at (a) $G = 287 \text{ kg/m}^2\text{s}$ and (b) $G = 431 \text{ kg/m}^2\text{s}$ -----	63
Fig. 4.12	Mean bubble departure frequencies for various coolant mass fluxes for $T_{\text{sat}} = 54.3 \text{ }^\circ\text{C}$ for the chip with (a) smooth surface and (b) pin-finned 200 Surface and (c) pin-finned 100 surface -----	64
Fig. 4.13	Mean bubble departure frequencies for various micro-structures of chip surface for $T_{\text{sat}} = 54.3 \text{ }^\circ\text{C}$ at (a) $G = 287 \text{ kg/m}^2\text{s}$ and (b) $G = 431 \text{ kg/m}^2\text{s}$ -----	65
Fig. 4.14	Mean active nucleation site densities for various coolant mass fluxes for $T_{\text{sat}} = 54.3 \text{ }^\circ\text{C}$ for the chip with (a) smooth surface and (b) pin-finned 200 Surface (c) pin-finned 100 Surface-----	66
Fig. 4.15	Mean active nucleation site densities for various micro-structures of chip surface for $T_{\text{sat}} = 54.3 \text{ }^\circ\text{C}$ at (a) $G = 287 \text{ kg/m}^2\text{s}$ and (b) $G = 431 \text{ kg/m}^2\text{s}$ -----	67
Fig. 4.16	Comparison of the measured data for Nusselt number for saturated flow boiling of FC-72 on smooth surface with the proposed correlation-----	68
Fig. 4.17	Comparison of the measured data for Nusselt number for saturated flow boiling of FC-72 on pin-finned surfaces with the proposed correlation-----	69
Fig. 4.18	Comparison of the measured data for mean bubble departure diameter for saturated flow boiling of FC-72 on smooth surface with the proposed correlation -----	70
Fig. 4.19	Comparison of the measured data for mean bubble departure diameter for saturated flow boiling of FC-72 on pin-finned surfaces with the proposed correlation -----	71

Fig. 4.20 Comparison of the measured data for mean bubble departure frequency for saturated flow boiling of FC-72 on smooth surface with the proposed correlation -----	72
Fig. 4.21 Comparison of the measured data for mean bubble departure frequency for saturated flow boiling of FC-72 on pin-finned surfaces with the proposed correlation -----	73
Fig. 4.22 Comparison of the measured data for mean active nucleation site density for saturated flow boiling of FC-72 on smooth surface with the proposed correlation -----	74
Fig. 4.23 Comparison of the measured data for mean active nucleation site density for saturated flow boiling of FC-72 on pin-finned surfaces with the proposed correlation -----	75
Fig. 4.24 Comparison of the measured data for boiling heat flux for saturated flow boiling of FC-72 on smooth surface with the proposed correlation-----	76
Fig. 4.25 Comparison of the measured data for boiling heat flux for saturated flow boiling of FC-72 on pin-finned surfaces with the proposed correlation-----	77

Subcooled Flow Boiling

Fig. 5.1 Boiling curves for the chip with smooth surface for various coolant mass fluxes at (a) $T_{sub} = 2.3 \text{ }^\circ\text{C}$ and (b) $T_{sub} = 4.3 \text{ }^\circ\text{C}$ -----	91
Fig. 5.2 Boiling curves for the chip with pin-finned 200 surface for various coolant mass fluxes at (a) $T_{sub} = 2.3 \text{ }^\circ\text{C}$ and (b) $T_{sub} = 4.3 \text{ }^\circ\text{C}$ -----	92
Fig. 5.3 Boiling curves for the chip with pin-finned 100 surface for various coolant mass fluxes at (a) $T_{sub} = 2.3 \text{ }^\circ\text{C}$ and (b) $T_{sub} = 4.3 \text{ }^\circ\text{C}$ -----	93
Fig. 5.4 Boiling curves for the chip with smooth surface for various inlet liquid subcoolings at (a) $G = 287 \text{ kg/m}^2\text{s}$ and (b) $G = 431 \text{ kg/m}^2\text{s}$ -----	94
Fig. 5.5 Boiling curves for the chip with pin-finned 200 surface for various inlet liquid subcoolings at (a) $G = 287 \text{ kg/m}^2\text{s}$ and (b) $G = 431 \text{ kg/m}^2\text{s}$ -----	95
Fig. 5.6 Boiling curves for the chip with pin-finned100 surface for various inlet liquid subcoolings at (a) $G = 287 \text{ kg/m}^2\text{s}$ and (b) $G = 431 \text{ kg/m}^2\text{s}$ -----	96
Fig. 5.7 Boiling curves affected by surface micro-structures for $T_{sub} = 2.3 \text{ }^\circ\text{C}$ at (a)	

	$G = 287 \text{ kg/m}^2\text{s}$ and (b) $G = 431 \text{ kg/m}^2\text{s}$ -----	97
Fig. 5.8	Boiling curves affected by surface micro-structures for $T_{\text{sub}} = 4.3 \text{ }^\circ\text{C}$ at (a) $G = 287 \text{ kg/m}^2\text{s}$ and (b) $G = 431 \text{ kg/m}^2\text{s}$ -----	98
Fig. 5.9	Subcooled flow boiling heat transfer coefficients for the chip with smooth surface for various coolant mass fluxes at (a) $T_{\text{sub}} = 2.3 \text{ }^\circ\text{C}$ and (b) T_{sub} $= 4.3 \text{ }^\circ\text{C}$ -----	99
Fig. 5.10	Subcooled flow boiling heat transfer coefficients for the chip with pin-finned 200 surface for various coolant mass fluxes at (a) $T_{\text{sub}} = 2.3 \text{ }^\circ\text{C}$ and (b) $T_{\text{sub}} = 4.3 \text{ }^\circ\text{C}$ -----	100
Fig. 5.11	Subcooled flow boiling heat transfer coefficients for the chip with pin-finned 100 surface for various coolant mass fluxes at (a) $T_{\text{sub}} = 2.3 \text{ }^\circ\text{C}$ and (b) $T_{\text{sub}} = 4.3 \text{ }^\circ\text{C}$ -----	101
Fig. 5.12	Subcooled flow boiling heat transfer coefficients for the chip with smooth surface for various inlet liquid subcoolings at (a) $G = 287 \text{ kg/m}^2\text{s}$ and (b) G $= 431 \text{ kg/m}^2\text{s}$ -----	102
Fig. 5.13	Subcooled flow boiling heat transfer coefficients for the chip with pin-finned 200 surface for various inlet liquid subcoolings at (a) $G = 287$ $\text{kg/m}^2\text{s}$ and (b) $G = 431 \text{ kg/m}^2\text{s}$ -----	103
Fig. 5.14	Subcooled flow boiling heat transfer coefficients for the chip with pin-finned 100 surface for various inlet liquid subcoolings at (a) $G = 287$ $\text{kg/m}^2\text{s}$ and (b) $G = 431 \text{ kg/m}^2\text{s}$ -----	104
Fig. 5.15	Subcooled flow boiling heat transfer coefficients affected by surface micro-structures for $T_{\text{sub}} = 2.3 \text{ }^\circ\text{C}$ at (a) $G = 287 \text{ kg/m}^2\text{s}$ and (b) $G = 431$ $\text{kg/m}^2\text{s}$ -----	105
Fig. 5.16	Subcooled flow boiling heat transfer coefficients affected by surface micro-structures for $T_{\text{sub}} = 4.3 \text{ }^\circ\text{C}$ at (a) $G = 287 \text{ kg/m}^2\text{s}$ and (b) $G = 431$ $\text{kg/m}^2\text{s}$ -----	106
Fig. 5.17	Photos of boiling flow for various imposed heat fluxes for the chip with smooth surface at $T_{\text{sub}} = 2.3 \text{ }^\circ\text{C}$ for (a) $G = 287 \text{ kg/m}^2\text{s}$ and (b) $G = 431$ $\text{kg/m}^2\text{s}$ -----	107

Fig. 5.18 Photos of boiling flow for various imposed heat fluxes for the chip with smooth surface at $T_{\text{sub}} = 4.3 \text{ }^{\circ}\text{C}$ for (a) $G = 287 \text{ kg/m}^2\text{s}$ and (b) $G = 431 \text{ kg/m}^2\text{s}$ -----	108
Fig. 5.19 Photos of boiling flow for various imposed heat fluxes for the chip with pin-finned 200 surface at $T_{\text{sub}} = 2.3 \text{ }^{\circ}\text{C}$ for (a) $G = 287 \text{ kg/m}^2\text{s}$ and (b) $G = 431 \text{ kg/m}^2\text{s}$ -----	109
Fig. 5.20 Photos of boiling flow for various imposed heat fluxes for the chip with pin-finned 200 surface at $T_{\text{sub}} = 4.3 \text{ }^{\circ}\text{C}$ for (a) $G = 287 \text{ kg/m}^2\text{s}$ and (b) $G = 431 \text{ kg/m}^2\text{s}$ -----	110
Fig. 5.21 Photos of boiling flow for various imposed heat fluxes for the chip with pin-finned 100 surface at $T_{\text{sub}} = 2.3 \text{ }^{\circ}\text{C}$ for (a) $G = 287 \text{ kg/m}^2\text{s}$ and (b) $G = 431 \text{ kg/m}^2\text{s}$ -----	111
Fig. 5.22 Photos of boiling flow for various imposed heat fluxes for the chip with pin-finned 100 surface at $T_{\text{sub}} = 4.3 \text{ }^{\circ}\text{C}$ for (a) $G = 287 \text{ kg/m}^2\text{s}$ and (b) $G = 431 \text{ kg/m}^2\text{s}$ -----	112
Fig. 5.23 Mean bubble departure diameters for subcooled flow boiling from smooth surface for various coolant mass fluxes at (a) $T_{\text{sub}} = 2.3 \text{ }^{\circ}\text{C}$ and (b) $T_{\text{sub}} = 4.3 \text{ }^{\circ}\text{C}$ -----	113
Fig. 5.24 Mean bubble departure diameters for subcooled flow boiling from pin-finned 200 surface for various coolant mass fluxes at (a) $T_{\text{sub}} = 2.3 \text{ }^{\circ}\text{C}$ and (b) $T_{\text{sub}} = 4.3 \text{ }^{\circ}\text{C}$ -----	114
Fig. 5.25 Mean bubble departure diameters for subcooled flow boiling from pin-finned 100 surface for various coolant mass fluxes at (a) $T_{\text{sub}} = 2.3 \text{ }^{\circ}\text{C}$ and (b) $T_{\text{sub}} = 4.3 \text{ }^{\circ}\text{C}$ -----	115
Fig. 5.26 Mean bubble departure diameters for subcooled flow boiling from smooth surface for various inlet liquid subcoolings at (a) $G = 287 \text{ kg/m}^2\text{s}$ and (b) $G = 431 \text{ kg/m}^2\text{s}$ -----	116
Fig. 5.27 Mean bubble departure diameters for subcooled flow boiling from pin-finned 200 surface for various inlet liquid subcoolings at (a) $G = 287 \text{ kg/m}^2\text{s}$ and (b) $G = 431 \text{ kg/m}^2\text{s}$ -----	117

Fig. 5.28 Mean bubble departure diameters for subcooled flow boiling from pin-finned 100 surface for various inlet liquid subcoolings at (a) $G = 287 \text{ kg/m}^2\text{s}$ and (b) $G = 431 \text{ kg/m}^2\text{s}$ -----	118
Fig. 5.29 Mean bubble departure diameters for subcooled flow boiling affected by surface micro-structures for $T_{\text{sub}} = 2.3 \text{ }^\circ\text{C}$ at (a) $G = 287 \text{ kg/m}^2\text{s}$ and (b) $G = 431 \text{ kg/m}^2\text{s}$ -----	119
Fig. 5.30 Mean bubble departure diameters for subcooled flow boiling affected by surface micro-structures for $T_{\text{sub}} = 4.3 \text{ }^\circ\text{C}$ at (a) $G = 287 \text{ kg/m}^2\text{s}$ and (b) $G = 431 \text{ kg/m}^2\text{s}$ -----	120
Fig. 5.31 Mean bubble departure frequencies for subcooled flow boiling from smooth surface for various coolant mass fluxes at (a) $T_{\text{sub}} = 2.3 \text{ }^\circ\text{C}$ and (b) $T_{\text{sub}} = 4.3 \text{ }^\circ\text{C}$ -----	121
Fig. 5.32 Mean bubble departure frequencies for subcooled flow boiling from pin-finned 200 surface for various coolant mass fluxes at (a) $T_{\text{sub}} = 2.3 \text{ }^\circ\text{C}$ and (b) $T_{\text{sub}} = 4.3 \text{ }^\circ\text{C}$ -----	122
Fig. 5.33 Mean bubble departure frequencies for subcooled flow boiling from pin-finned 100 surface for various coolant mass fluxes at (a) $T_{\text{sub}} = 2.3 \text{ }^\circ\text{C}$ and (b) $T_{\text{sub}} = 4.3 \text{ }^\circ\text{C}$ -----	123
Fig. 5.34 Mean bubble departure frequencies for subcooled flow boiling from smooth surface for various inlet liquid subcoolings at (a) $G = 287 \text{ kg/m}^2\text{s}$ and (b) $G = 431 \text{ kg/m}^2\text{s}$ -----	124
Fig. 5.35 Mean bubble departure frequencies for subcooled flow boiling from pin-finned 200 surface for various inlet liquid subcoolings at (a) $G = 287 \text{ kg/m}^2\text{s}$ and (b) $G = 431 \text{ kg/m}^2\text{s}$ -----	125
Fig. 5.36 Mean bubble departure frequencies for subcooled flow boiling from pin-finned 100 surface for various inlet liquid subcoolings at (a) $G = 287 \text{ kg/m}^2\text{s}$ and (b) $G = 431 \text{ kg/m}^2\text{s}$ -----	126
Fig. 5.37 Mean bubble departure frequencies for subcooled flow boiling affected by surface micro-structures for $T_{\text{sub}} = 2.3 \text{ }^\circ\text{C}$ at (a) $G = 287 \text{ kg/m}^2\text{s}$ and (b) $G = 431 \text{ kg/m}^2\text{s}$ -----	127

Fig. 5.38 Mean bubble departure frequencies for subcooled flow boiling affected by surface micro-structures for $T_{\text{sub}} = 4.3 \text{ }^\circ\text{C}$ at (a) $G = 287 \text{ kg/m}^2\text{s}$ and (b) $G = 431 \text{ kg/m}^2\text{s}$ -----	128
Fig. 5.39 Mean active nucleation site densities for subcooled flow boiling from smooth surface for various coolant mass fluxes at (a) $T_{\text{sub}} = 2.3 \text{ }^\circ\text{C}$ and (b) $T_{\text{sub}} = 4.3 \text{ }^\circ\text{C}$ -----	129
Fig. 5.40 Mean active nucleation site densities for subcooled flow boiling from pin-finned 200 surface for various coolant mass fluxes at (a) $T_{\text{sub}} = 2.3 \text{ }^\circ\text{C}$ and (b) $T_{\text{sub}} = 4.3 \text{ }^\circ\text{C}$ -----	130
Fig. 5.41 Mean active nucleation site densities for subcooled flow boiling from pin-finned 100 surface for various coolant mass fluxes at (a) $T_{\text{sub}} = 2.3 \text{ }^\circ\text{C}$ and (b) $T_{\text{sub}} = 4.3 \text{ }^\circ\text{C}$ -----	131
Fig. 5.42 Mean active nucleation site densities for subcooled flow boiling from smooth surface for various inlet liquid subcoolings at (a) $G = 287 \text{ kg/m}^2\text{s}$ and (b) $G = 431 \text{ kg/m}^2\text{s}$ -----	132
Fig. 5.43 Mean active nucleation site densities for subcooled flow boiling from pin-finned 200 surface for various inlet liquid subcoolings at (a) $G = 287 \text{ kg/m}^2\text{s}$ and (b) $G = 431 \text{ kg/m}^2\text{s}$ -----	133
Fig. 5.44 Mean active nucleation site densities for subcooled flow boiling from pin-finned 100 surface for various inlet liquid subcoolings at (a) $G = 287 \text{ kg/m}^2\text{s}$ and (b) $G = 431 \text{ kg/m}^2\text{s}$ -----	134
Fig. 5.45 Mean active nucleation site densities for subcooled flow boiling affected by surface micro-structures for $T_{\text{sub}} = 2.3 \text{ }^\circ\text{C}$ at (a) $G = 287 \text{ kg/m}^2\text{s}$ and (b) $G = 431 \text{ kg/m}^2\text{s}$ -----	135
Fig. 5.46 Mean active nucleation site densities for subcooled flow boiling affected by surface micro-structures for $T_{\text{sub}} = 4.3 \text{ }^\circ\text{C}$ at (a) $G = 287 \text{ kg/m}^2\text{s}$ and (b) $G = 431 \text{ kg/m}^2\text{s}$ -----	136
Fig. 5.47 Comparison of the measured data for Nusselt number for subcooled flow boiling of FC-72 on smooth surface with the proposed correlation-----	137
Fig. 5.48 Comparison of the measured data for Nusselt number for subcooled flow	

boiling of FC-72 on pin-finned surfaces with the proposed correlation-----	138
Fig. 5.49 Comparison of the measured data for mean bubble departure diameter for subcooled flow boiling of FC-72 on smooth surface with the proposed correlation -----	139
Fig. 5.50 Comparison of the measured data for mean bubble departure diameter for subcooled flow boiling of FC-72 on pin-finned surfaces with the proposed correlation -----	140
Fig. 5.51 Comparison of the measured data for mean bubble departure frequency for subcooled flow boiling of FC-72 on smooth surface with the proposed correlation -----	141
Fig. 5.52 Comparison of the measured data for mean bubble departure frequency for subcooled flow boiling of FC-72 on pin-finned surfaces with the proposed correlation -----	142
Fig. 5.53 Comparison of the measured data for mean active nucleation site density for subcooled flow boiling of FC-72 on smooth surface with the proposed correlation -----	143
Fig. 5.54 Comparison of the measured data for mean active nucleation site density for subcooled flow boiling of FC-72 on pin-finned surfaces with the proposed correlation -----	144
Fig. 5.55 Comparison of the measured data for boiling heat flux for subcooled flow boiling of FC-72 on smooth surface with the proposed correlation-----	145
Fig. 5.56 Comparison of the measured data for boiling heat flux for subcooled flow boiling of FC-72 on pin-finned surfaces with the proposed correlation-----	146

NOMENCLATURE

A	area, m ²
B	fin height, m
Bo	Boiling number, $Bo = \frac{q}{G \cdot i_{fg}}$, dimensionless
c_p	specific heat, J/kg
D	hydraulic diameter of rectangular-channel, m
E	enhancement factor
F	pin-fin factor for the effects of fin geometries, dimensionless
Fr	Froude number, $Fr_1 = \frac{G^2}{\rho_l^2 \cdot g \cdot D_h}$, dimensionless
G	mass flux, kg/m ² s
g	acceleration due to gravity, m ² /s
H	height, m
h	heat transfer coefficient, W/m ² ·K
I	measured current from DC power supply, A
i_{lv}	enthalpy of vaporization, J/kg·K
Ja	Jacob number based on ΔT_{sat} , $Ja = \frac{\rho_l \cdot C_{pl} \cdot \Delta T_{sat}}{\rho_v \cdot i_{lv}}$, dimensionless
Ja'	Jacob number based on ΔT_{sub} , $Ja' = \frac{\rho_l \cdot C_{pl} \cdot \Delta T_{sub}}{\rho_v \cdot i_{lv}}$, dimensionless
k	thermal conductivity, W/m·K
L	length, mm
\dot{m}	mass flow rate, kg/s
N	number of micro-pin-fins
N_{ac}	Active nucleation site density, n/m ²
N_{conf}	Confinement number, $N_{conf} = \frac{(\sigma/g \cdot \Delta\rho)^{0.5}}{D_h}$, dimensionless

Nu	Nusselt number, $Nu = \frac{h \cdot L}{k}$, dimensionless
P	system pressure, kPa
Pr	Prandtl number, $Pr = \frac{\mu \cdot C_p}{k}$, dimensionless
Q	heat transfer rate, W
q"	average imposed heat flux, W/cm ²
R	resistance of the electric-heater
Re	Reynolds number, $Re = \frac{G \cdot D}{\mu}$, dimensionless
S	fin space between two adjacent fins, m
T	temperature,
V	coolant FC-72 flow velocity, m/s
V	measured voltage from DC power supply, V
W	width, m



Greek Symbols

ΔT	temperature difference,
ρ	density, kg/m ³
μ	dynamic viscosity, N·s/m ²
v	specific volume, m ³ /kg
σ	surface tension, N/m
α	void fraction, dimensionless
ε	relative heat loss, dimensionless
ϕ	contact angle
ϕ_s	static contact angle

Subscripts

ave	average
c,h	from heater surface to cooper surface
chip	chip surface
cop	copper
cs	cross-section of rectangular-channel
d	diameter
e	effective
f	fin
fin	mean bubble departure frequency
g	gas
h	hydraulic
i	at the inlet of the test section
in	at the inlet of the test section
i,o	at inlet and exit of the test section
l	all-liquid nonboiling heat transfer
lv	liquid phase to vapor phase
m	average value for the two phase mixture or between the inlet and exit
mica	mica
n	net power input to the coolant FC-72
n	active nucleation site density
o	at the outlet of the test section
p	preheater
pool	pool boiling
r	coolant FC-72
s	surface
sat	saturated state for coolant FC-72

sp	single-phase convective heat transfer
sub	subcooled state for coolant FC-72
t	total
t-g	thermal-grease
tp	two-phase boiling heat transfer
v	vapor
w	wall
w	water
1ϕ	single-phase
2ϕ	two-phase

